remote sensing

MDPI

Communication

Moisture Content Vegetation Seasonal Variability Based on a Multiscale Remote Sensing Approach

Filippe L. M. Santos [1,2,*], Gonçalo Rodrigues [1,2], Miguel Potes [1,2,3], Flavio T. Couto [1,2,3], Maria João Costa [1,2,3], Susana Dias [4], Maria José Monteiro [5], Nuno de Almeida Ribeiro [1,6] and Rui Salgado [1,2,3]

1 Instituto de Ciências da Terra (ICT), Instituto de Investigação e Formação Avançada (IIFA), Universidade de Évora, Rua Romão Ramalho, 59, 7000-671 Évora, Portugal; grodrigues@uevora.pt (G.R.); mpotes@uevora.pt (M.P.); fcouto@uevora.pt (F.T.C.); mjcosta@uevora.pt (M.J.C.); nmcar@uevora.pt (N.d.A.R.); rsal@uevora.pt (R.S.)
2 Earth Remote Sensing Laboratory (EaRSLab), Universidade de Évora, Rua Romão Ramalho, 7000-671 Évora, Portugal
3 Departamento de Física, Escola de Ciências e Tecnologia (ECT), Universidade de Évora, Rua Romão Ramalho, 7000-671 Évora, Portugal
4 VALORIZA—Research Centre for Endogenous Resource Valorization, Instituto Politécnico de Portalegre, 7300-110 Portalegre, Portugal; sdias@ipportalegre.pt
5 Instituto Português do Mar e da Atmosfera I.P., Rua C do Aeroporto, 1749-077 Lisboa, Portugal; maria.monteiro@ipma.pt
6 Departamento de Fitotecnia, Escola de Ciências e Tecnologia (ECT), Universidade de Évora, Pólo da Mitra Ap. 94, 7002-554 Évora, Portugal
* Correspondence: filippe.santos@uevora.pt

Abstract: Water content is one of the most critical characteristics in plant physiological development. Therefore, this information is a crucial factor in determining the water stress conditions of vegetation, which is essential for assessing the wildfire risk and land management decision-making. Remote sensing can be vital for obtaining information over large, limited access areas with global coverage. This is important since conventional techniques for collecting vegetation water content are expensive, time-consuming, and spatially limited. This work aims to evaluate the vegetation live fuel moisture content (LFMC) seasonal variability using a multiscale remote sensing approach, particularly on rockroses, the *Cistus ladanifer* species, a Western Mediterranean basin native species with wide spatial distribution, over the Herdade da Mitra at the University of Évora, Portugal. This work used four dataset sources, collected monthly between June 2022 and July 2023: (i) Vegetation samples used to calculate the LFMC; (ii) Vegetation reflectance spectral signature using the portable spectroradiometer FieldSpec HandHeld-2 (HH2); (iii) Multispectral optical imagery obtained from the Multispectral Instrument (MSI) sensor onboard the Sentinel-2 satellite; and (iv) Multispectral optical imagery derived from a camera onboard an Unmanned Aerial Vehicle Phantom 4 Multispectral (P4M). Several temporal analyses were performed based on datasets from different sensors and on their intercomparison. Furthermore, the Random Forest (RF) classifier, a machine learning model, was used to estimate the LFMC considering each sensor approach. MSI sensor presented the best results (R^2 = 0.94) due to the presence of bands on the Short-Wave Infrared Imagery region. However, despite having information only in the Visible and Near Infrared spectral regions, the HH2 presents promising results (R^2 = 0.86). This suggests that by combining these spectral regions with a RF classifier, it is possible to effectively estimate the LFMC. This work shows how different spatial scales, from remote sensing observations, affect the LFMC estimation through machine learning techniques.

Keywords: LFMC; remote sensing; UAV; Sentinel-2; Fieldspec; Random Forest

Citation: Santos, F.L.M.; Rodrigues, G.; Potes, M.; Couto, F.T.; Costa, M.J.; Dias, S.; Monteiro, M.J.; Ribeiro, N.d.A.; Salgado, R. Moisture Content Vegetation Seasonal Variability Based on a Multiscale Remote Sensing Approach. *Remote Sens.* **2024**, *16*, 4434. https://doi.org/10.3390/rs16234434

Academic Editors: Paulo Jose Murillo-Sandoval, Li Zhao, Colleen Bryant and Nicolas Younes

Received: 19 September 2024
Revised: 15 November 2024
Accepted: 20 November 2024
Published: 27 November 2024

1. Introduction

Wildfires are a vital component in the dynamics of the Earth system, with important socioeconomic activities impacting around the globe, such as forest degradation, land use changes, atmospheric emissions, and, in some cases, human losses [1]. Fire activity is highly related to fuel availability, weather conditions, ignition agents and human activity [2]. In future climate scenarios, warmer and drier conditions are expected across the globe, but with some specific hotspots. For the Iberian Peninsula, an increase in the number and extension of extreme event episodes is expected, particularly heat waves [3]. These extreme events have led to an increase in the number of drought years, increasing the amount of flammable material available to burn and, consequently, extending the fire season [4,5].

In this context, the knowledge of vegetation spatial and temporal distribution, namely canopy height, above ground biomass and fuel moisture content, is essential for wildfire risk assessment, as it is a critical factor in landscape management to combat forest fires. In order to fill this lack of knowledge, research in this field has been stepped up in recent years, mainly on regional scales, due to the extensive variability of geomorphological characteristics, vegetation heterogeneity and species diversity [6,7].

Fuel moisture content (FMC) represents the water content within vegetation and plays a pivotal role in determining wildfire occurrence and behaviour. Usually, FMC is separated into live (LFMC) and dead (DFMC) constituents. Both FMCs are highly significant to wildfire ignition and propagation [8], and consequently in modelling the spread of fires, particularly through coupled atmosphere-fire models [9]. Dead leaves and branches could burn quickly, increasing fire spread, while live fuel can reduce fire spread due to its water content. Based on phenology mechanisms, live plants can adapt to stress conditions, which correlate more with local biophysical and geomorphological factors than weather conditions, making it extremely difficult to estimate the LFMC [10].

Although LFMC measurements are essential, fieldwork campaigns are time-consuming and space-limited, making continuous large-scale monitoring unfeasible [8,11,12]. Remote sensing stands out as an efficient approach to provide systematic, wide-ranging, helpful information about vegetation parameters. Several studies spotlight different characteristics of satellite capabilities for predicting LFMC [13–16]. However, fewer studies emphasize the estimation of LFMC using spectral information in the visible and infrared electromagnetic spectrum, ranging between 400 and 1000 nm, like unmanned aerial vehicle (UAV) with commercial cameras [17,18].

In the literature, there are studies that combine multiple spatial and spectral scales in applications across various research fields, such as mineral classification [19], plant functional classification in the Arctic [20], and vegetation monitoring [21]. However, none have applied this approach for long term LFMC monitoring.

Furthermore, recent studies have been published in which machine learning techniques combined with remote sensing data are used to develop models and products, yielding promising results [13,22–25]. Random Forest (RF) is a simple model that adds machine learning with low computational cost, and great efficiency in solving regression and classification problems. RF is a statistical classifier that is data-driven, non-parametric, based on a tree structure, and can be applied to classification or regression tasks [26].

Remote sensing information derived from Sentinel-2 satellite multispectral imagery, UAV multispectral imagery and field spectroradiometer spectral signatures obtained during fieldwork were combined with vegetation LFMC field samples. Samples were obtained over shrubland areas, particularly in the *Cistus ladanifer* species presence, since it is native to the western Mediterranean basin and has a wide spatial distribution over Portugal [27]. This work aims to evaluate the LFMC's seasonal temporal variability using multiscale remote sensing approaches, i.e., using different sensors, to analyze the reflectance impact due to scale over the LFMC behaviour. In this sense, a secondary objective was to evaluate how the spectral information, derived from different multiscale sensor acquisitions and used as predictor parameters in a RF classifier, can effectively estimate the LFMC variable.

The work is organized as follows: Section 2 describes the study area, datasets, and the methodology used. Results and discussions are presented in Section 3. Finally, the conclusions and directions for future research are summarized in Section 4.

2. Materials and Methods

2.1. Study Area

The study area (Figure 1) is located within the Herdade da Mitra facilities, one pole of the University of Évora. The area has 290 ha, and agriculture is the main occupation, including cork oak, holm oak, bushes and pastures, parcels of olive groves, pine forests and vineyards. The Herdade da Mitra is considered a living laboratory of inestimable value for the research and teaching activities of the University of Évora, being a unique hotspot that has never been seen anywhere in the world. [28,29]. The area used in this work is located on a hill covered by shrublands, especially *Cistus ladanifer* species. This abundant bush species over the Iberian Peninsula and the Mediterranean basin has a high flammability capacity throughout the year [27]. This area is typical of southern portions of Portugal, with cork and holm oak mosaics and silviculture, agriculture, and livestock activities that provide rich environmental value for the region.

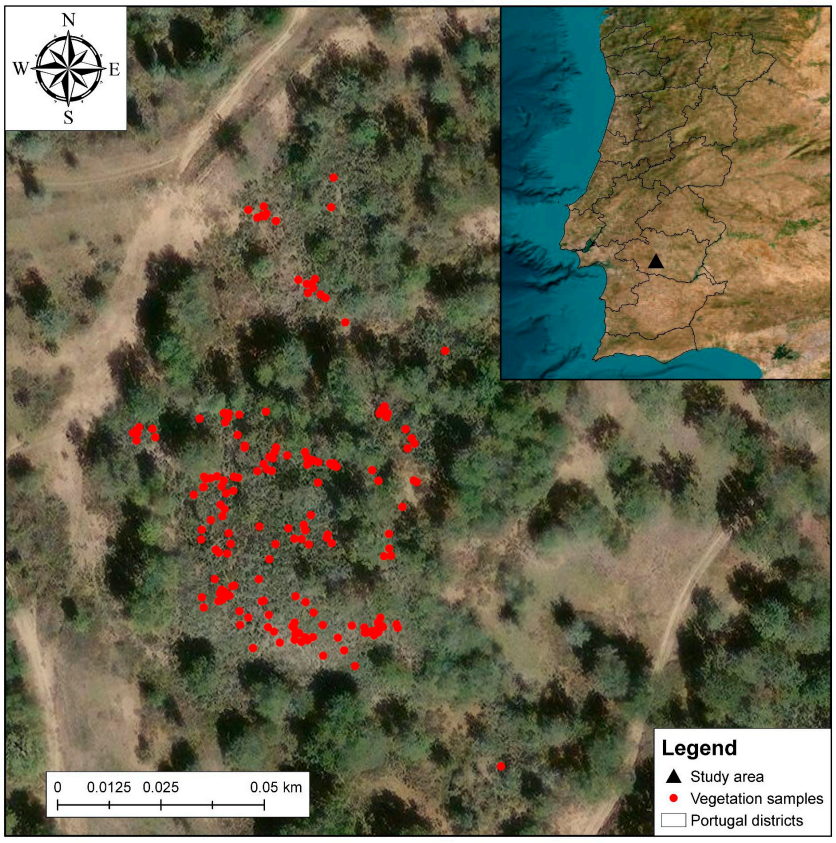

Figure 1. Study area: Herdade da Mitra site, Évora (black triangle). The red dots indicate the locations where vegetation samples used in this study were collected.

2.2. Data

2.2.1. In-Situ LFMC Data

The vegetation moisture content estimates, particularly LFMC, consisted of leaf field samples collected in hermetically sealed bags. At the same time, the geographic coordinate point is recorded using a Global Navigation Satellite System (GNSS) data receiver device. The field samples were transported to the laboratory, weighed, and dried in an oven at 105 °C for 24 h. The LFMC is estimated based on the difference between the weight before

and after drying. This methodology is the widely used and well established [30]. The LFMC database derived from fieldwork campaigns was stored on the Zenodo data repository [31].

2.2.2. Unmanned Aerial Vehicle (UAV) Data

Multispectral optical imagery was derived from a multispectral camera onboard a Da-Jiang Innovations (DJI) Phantom 4 Multispectral (P4M) UAV. The camera has five bands: blue (450 nm), green (560 nm), red (650 nm), near red (730 nm) and near-infrared (840 nm). The spatial resolution is defined once the flight height is configured. In this case, the flight was carried out at a height of 120 m and the ground sample distance was 6 cm/pixel. The surveys were carried out near 1100 UTC, close to the satellite overpass.

For post-processing, the software used to process imagery was the Pix4DMapper 4.7.5, which allows the completion of all workflow steps for UAV imagery processing. The main steps are (i) keypoint extraction, (ii) keypoint matching, (iii) aligning photos, (iv) geolocation, (v) point cloud dense generation, (vi) 3d texture mesh, (vii) Digital Surface Model (DSM), (viii) Orthomosaic, (ix) Reflectance map and, (x) Index map. In step (ix), on the conversion from digital number (DN) to reflectance, a Calibrated Reflectance Panel was used. The calibration reflectance panel consists of a grey or white panel on which the reflectance value of a plate is known for each wavelength. Thus, images over the calibration reflectance panel were recorded for the calibration step before, during, and after the UAV flight. It is important to highlight that the imagery generated by the UAV was not atmospherically corrected, since the flight height is only 120 m.

2.2.3. Satellite Data

Optical imagery derived from the Multispectral Instrument (MSI) sensor aboard the two Sentinel-2 mission satellites was used. The Copernicus Sentinel-2 mission comprises a constellation of two polar-orbiting satellites monitoring land surface variability with a 5-day revisit over the study area. MSI sensor has 12 bands with spatial resolution between 10 and 60 m. The collection used was Sentinel-2 Level-2A, which means surface reflectance, computed by sen2cor processing, i.e., atmospheric, terrain and cirrus correction from Top-Of-Atmosphere were performed [32]. For data extraction, the Google Earth Engine (GEE) platform was used. The platform has an extensive dataset image catalogue and simplifies processing steps and data manipulation, reducing time consumption [33]. The steps mosaicking, reprojection for WGS84 (EPSG 4326), and resampling for 20 m resolution by the nearest neighbor method were performed before the download step.

2.2.4. Field Spectroradiometer Data

The portable spectroradiometer FieldSpec HandHeld-2 (HH2), from Analytical Spectral Devices, Inc. is an UV/VNIR hyperspectral radiometer, which covers the spectral range 325–1075 nm, with a spectral resolution of 1 nm [34,35], used here to acquire hyperspectral reflectance measurements. Surface reflectance was determined as the ratio of the energy reflected by the sample to the energy incident on it, which was obtained by measuring a white calibration reference panel. To ensure consistency on lighting conditions, the sample measurements were taken immediately after the white reference measurement. The ViewSpecPro 6.2.0 software was used to streamline the measurement configuration parameters, including integration time, wavelength range, reflectance mode selection and sequential acquisition of multiple spectral measurements. This software facilitated the individual spectral file transfer into a format suitable for further processing in Python, ensuring an efficient and organized data processing workflow.

For each sample point, 60 reflectance spectral signatures were obtained in situ, reducing the errors and variations associated with the measurement. Usually, eight sample points were recorded for each date. Thereafter, a median of all reflectance spectral signatures for each date was considered on this work.

2.2.5. Meteorological Data

Weather information was also derived from a meteorological station located near the study area belonging to the Institute of Earth Sciences (ICT), Évora Pole. The ICT is responsible for the Herdade de Mitra meteorological station that is closely located to the study area. Daily mean air temperature, daily mean relative humidity and daily accumulated precipitation variables between January 2022 and July 2023 were used in this study.

2.3. Methods

We used field data collected over the study area from June 2022 to July 2023, covering all seasons of the year. The fieldwork dates were 28 June 2022, 28 July 2022, 22 August 2022, 26 September 2022, 27 October 2022, 25 November 2022, 28 February 2023, 14 April 2023 and 28 July 2023. During each campaign and for each point, a vegetation sample was collected to estimate the LFMC, and spectral information derived from each sensor (HH2, MSI and P4M) was retrieved.

In order to minimize the errors associated with differences in measurement time, the P4M surveys were, in general, carried out between 1000 and 1200 UTC. Immediately after the UAV flight, the field measurements and collection were performed. Also, on UAV and field measurements, grey and white reference panels were used to calculate the adjusted reflectance, respectively. In this work, different spatio-temporal analyses were carried out. First, seasonal variability analysis was evaluated based on meteorological variables over the study area. Second, an NDVI spatio-temporal analysis was generated based on orthophoto imagery obtained by the P4M sensor over the study region. Third, the vegetation spectral reflectance signatures temporal variability analysis was obtained from HH2 measurements. Finally, an intercomparison between the vegetation spectral reflectance signature and temporal variability from the three different sensors used is done: HH2, MSI and P4M.

Lastly, the Random Forest classifier was used in this study to predict the LFMC variable. It was selected for its simplicity, resistance to outliers, steadiness, and resilience to noise, despite the complexity and high demand for computational power and resources. Refs. [36,37] provides a detailed description of the theory. In summary, the RF model is constructed by repeatedly creating decision trees, using an input data random subset for each tree.

With the aim to predict each variable, training and testing data groups were generated, splitting the samples into 80% and 20% for training and testing, respectively. The RF model performance was evaluated taking into account statistical parameters like the Root Mean-Square Error (RMSE), Mean Absolute Error (MAE), and R^2. The MAE calculates the error size between the observed and predicted values, whereas the RMSE considers the square root of the errors. The R^2 measures the correlation between the observed and predicted values. These parameters help to evaluate how the model fits based on the data.

Three models based on data from each sensor (HH2, MSI and P4M) were developed as predictor variables for the RF classification. For the P4M and MSI sensors, all available spectral bands were used, i.e., 5 and 12 bands, respectively. For the HH2 sensor, spectral bands were used every 5 nm, instead of every 1 nm, to avoid introducing additional data that does not aggregate value for the RF classification.

3. Results and Discussion

3.1. Weather Conditions

Figure 2 shows the weather variables: monthly mean air temperature (black lines), monthly accumulated precipitation (blue bars), monthly mean relative humidity (grey lines), and monthly mean LFMC (green dots). It is possible to observe that the highest temperature values occurred, as expected, during the summer, with the maximum recorded in August 2022, and a decrease towards the winter season where it reached values near 10 °C.

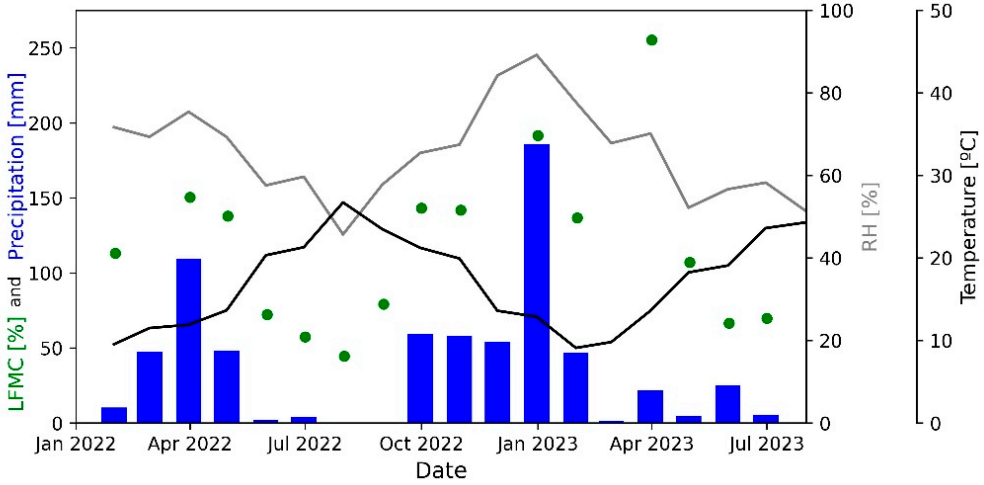

Figure 2. Meteorological variables over the study area: monthly mean air temperature (black), monthly accumulated precipitation (in blue) and monthly mean relative humidity (grey), whereas monthly LFMC (green dots) for the period between January 2022 and July 2023.

The two greatest precipitation windows occurred in April 2022 and from October 2022 to February 2023, with a maximum peak in January 2023, exceeding 170 mm. On the other hand, the LFMC values show the lowest values for summer due to drought conditions over vegetation, which are associated with higher temperatures, lower relative humidity and reduced precipitation during this period. As rain occurs, LFMC values increase, peaking at the end of autumn and spring.

These LFMC seasonal patterns observed here agree with results found by [38,39], who also study the seasonal variation of LFMC over shrubs in the Mediterranean basin, even considering other shrub species. In the study region, the drought conditions coincide with an increase in fuel dryness from May to October. This is characterized by high temperatures and low relative humidity at the surface, combined with a significant lack of precipitation during these months, leading to a substantial soil moisture deficit [40]. The LFMC values found present inverse patterns for temperature and similar for relative humidity/precipitation, i.e., as the temperature increases, the LFMC values decrease, whereas when relative humidity is high or it rains, the LFMC increases. This was expected as water infiltrates the plant, the vegetation water content and soil humidity will increase. [41] also showed the same seasonal LFMC behaviour, with the seasons regulating the LFMC variability, being modulated by meteorological variables.

3.2. Spatial and Temporal Distribution

Multispectral images derived from the P4M allowed a spatio-temporal characterization over the study area. Figure 3 shows the vegetation health evolution through the Normalized Difference Vegetation Index (NDVI), derived from P4M flights. NDVI is widely used in remote sensing studies and has several applications, especially in agriculture. NDVI is determined through a normalized difference between the near-infrared and red bands and is used to assess the vegetation health [42]. The highest NDVI values, represented by the blue color in the figure, indicate the higher vegetation photosynthetic activity due to higher photosynthesis, since chlorophyll is responsible for vegetation greenness. Therefore, it can be noted that the winter period presents higher NDVI values, while in summer, lower NDVI values are found, caused by high temperatures, low relative humidity and precipitation rates and consequently drier vegetation.

These results are corroborated with [43] findings, which show NDVI two-year time-series for six field plots derived from MSI sensor from Sentinel-2 over the southern region of Portugal. The study presents NDVI seasonal temporal variability with minimum values occurring in August 2023 and July 2024, whereas the maximum values are in November

2023, which agrees with the LFMC seasonal cycle. Regarding spatial variability, high NDVI values are associated with trees, while lower values are related to bare lands. Shrublands presented intermediate NDVI values. As trees and bushes lose their leaves, the visible green area becomes smaller, reducing NDVI values.

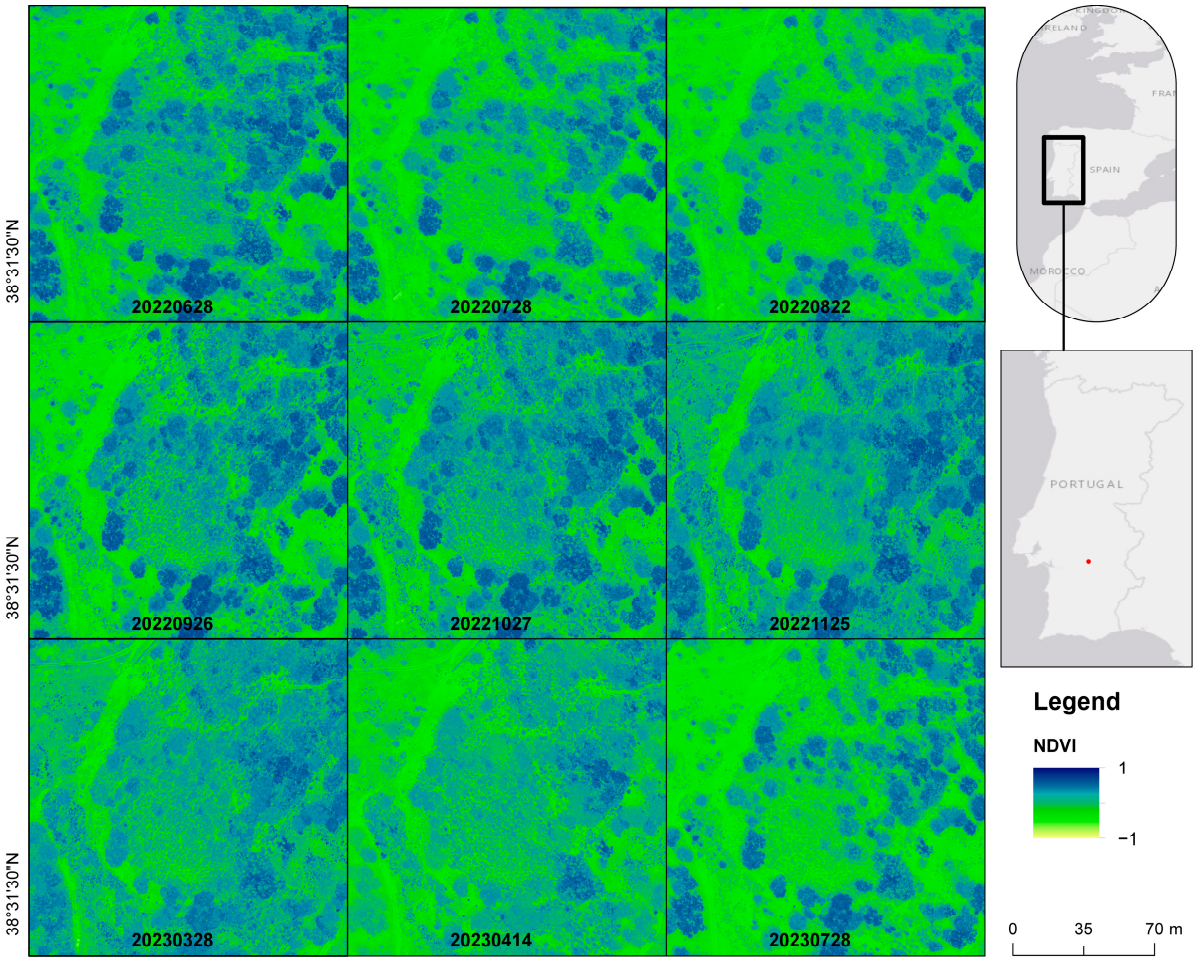

Figure 3. NDVI maps over the study area obtained from P4M measurements for each fieldwork (the date is indicated in each image).

UAV-derived NDVI mapping is widely used for agricultural purposes [44], as it allows on-demand monitoring of limited areas at sub-metric scales, avoiding dependence on other products, such as satellite imagery, which requires advanced knowledge and expensive field visits. Therefore, the information obtained through P4M is essential for understanding vegetation dynamics with high spatial resolution since it is possible to obtain images at centimetre-scale resolutions, distinguishing areas of scrubland from forest stands.

In Figure 4, the spectral signature measurement results reveal higher vegetation reflectance variability in the near-infrared spectral bandwidth. It is possible to observe lower reflectance values during the summer, and an increase in winter due to vegetation growth over the rainy months and reaching maximum values in spring (Figure 4a). Figure 4b shows the difference between the spectral signatures for each date and the average spectral signature. The reflectance values in the near-infrared range present negative values when compared to the average spectral signature during the summer months (June, July, and August). On the other hand, November, February, and April reflectance values present positive anomalies with values above 0.02. During the other months, reflectance values are close to the average spectral signature.

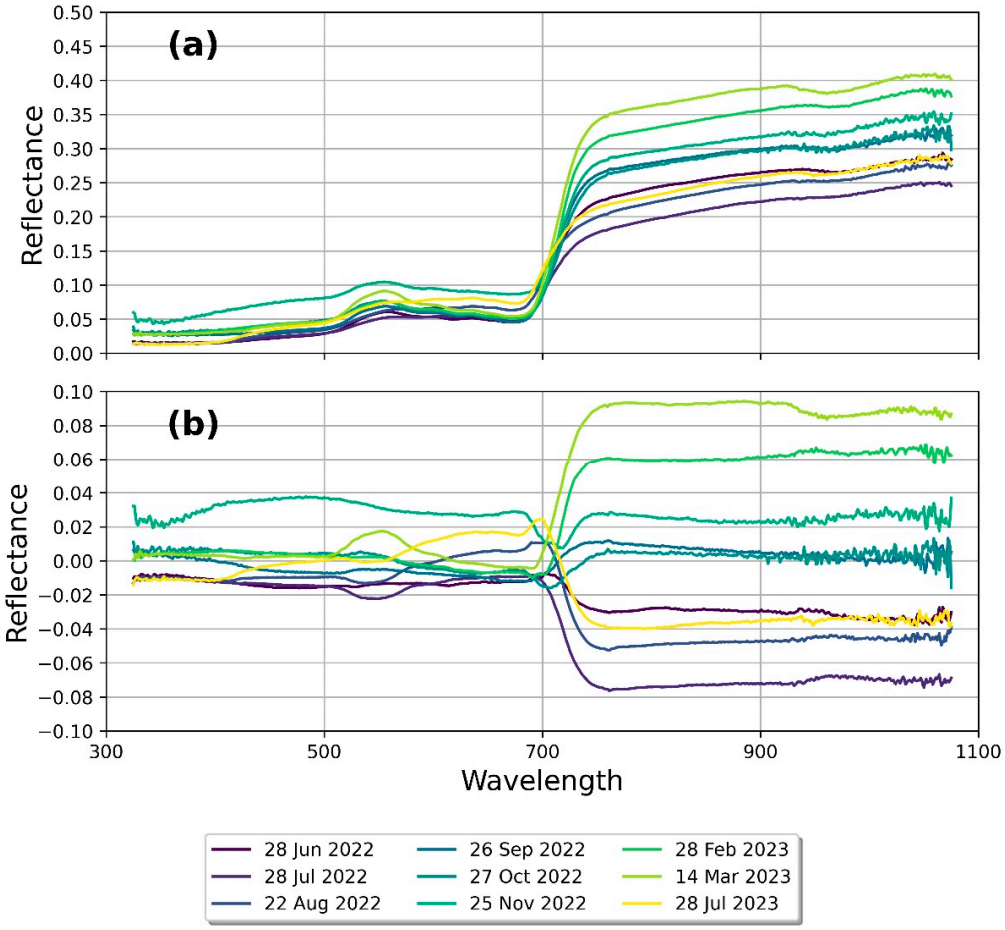

Figure 4. (**a**) Vegetation spectral signature obtained during the fieldwork campaigns derived from HH2 sensor. (**b**) Anomaly between the reflectance spectral signature for each date and the average reflectance spectral signature.

Figure 5 shows the intercomparison between different spectral sensors: HH2 (black line), MSI on board the Sentinel-2 satellite (green) and P4M (blue). It is worth mentioning that the data from the MSI sensor is the surface reflectance data already processed through the GEE platform. HH2 can offer thorough spectral reflectance data by measuring spectral information with a 1 nm resolution. Nonetheless, MSI and P4M operate with multispectral cameras that capture data through spectral bands, enabling information collection within specific electromagnetic spectrum ranges. During summer, there is a high correspondence between the reflectance values of all sensors, which is not observed in the following months.

The near-infrared reflectance's from HH2 are much higher than obtained by MSI and P4M. In some cases, even double the reflectance values, as verified on 27 October 2022 and 14 April 2023. One hypothesis that may partially explain this difference is the spatial scale of the different collections used in this study where the measurements with the HH2 were performed at the plant leaf level, while P4M and MSI had a spatial resolution of 6 cm and 20 m, respectively. This difference in spatial resolution causes the reflectance values measured by these sensors to be influenced by surrounding objects, potentially leading to reduced reflectance values. When comparing the P4M and MSI sensors, there are many days when the measured reflectance values are coherent. In addition, there are days in which the reflectance values of the P4M, especially in the near-infrared range, are lower than the MSI. This may be associated with the sensors' different spectral response functions, which causes the electromagnetic radiation captured by the sensors to be different, changing the reflectance values.

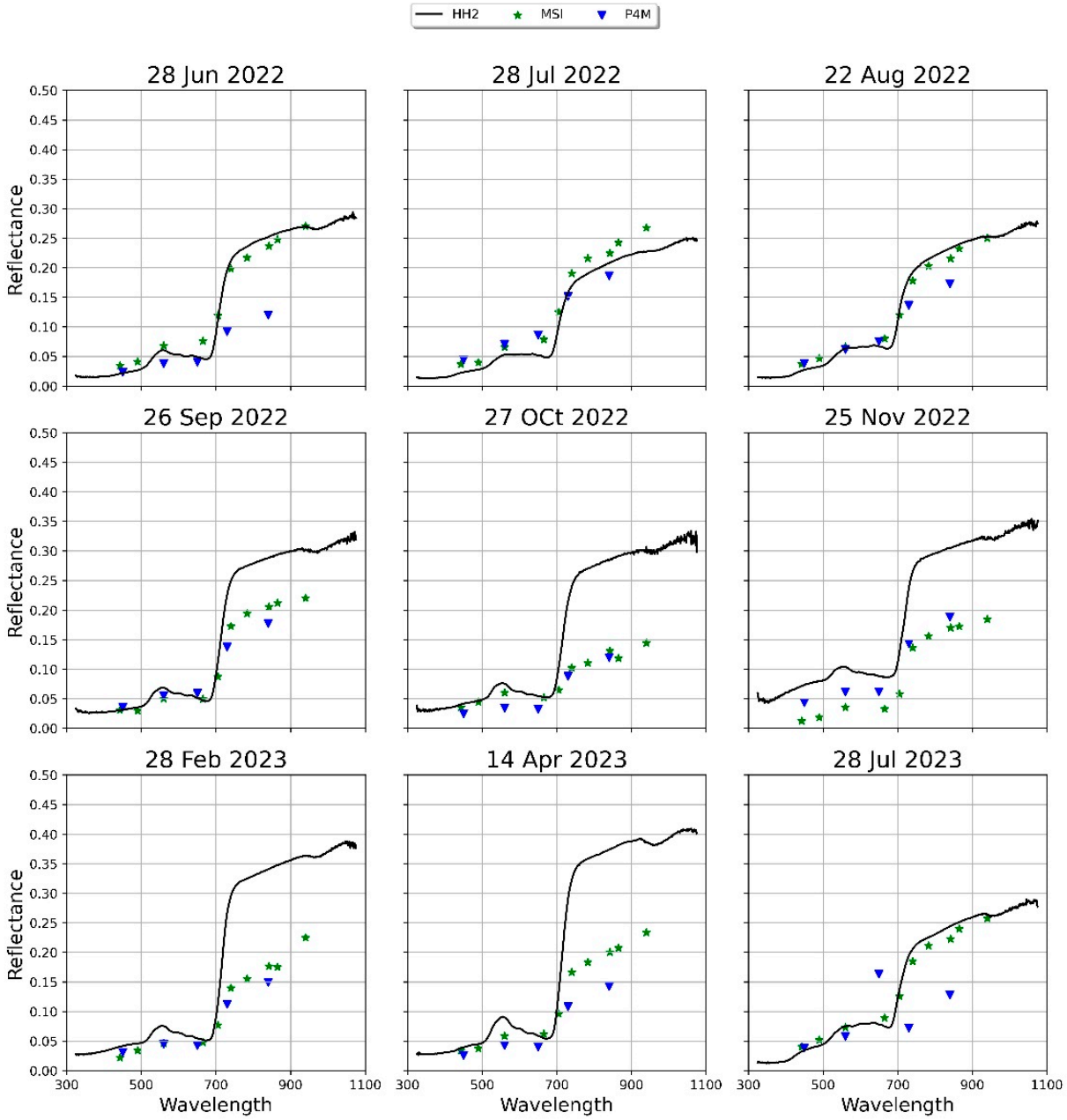

Figure 5. Spectral reflectance considering different sensors: HH2 (black), MSI (green) and P4M (blue).

3.3. Random Forest Classification

The performance of RF classifiers for each sensor in estimating vegetation LFMC was assessed. The model MSI-RF uses Sentinel-2 bands as a predictor and presented the best results, with R^2 of 0.94, higher than the model based on HH2 (0.86) and P4M (0.72) (Figure 6). Regarding RMSE and MAE values over different sensors, the MSI RF model obtained the best results with 17% and 11%, respectively. Whereas the HH2 and P4M presented values above 25% and 17% for RMSE and MAE, respectively.

It is worth mentioning that the MSI sensor has two bands in the SWIR region, B11 (1610 nm) and B12 (2190 nm). This region has greater sensitivity to water content, increasing the model performance in estimating the LFMC [45].

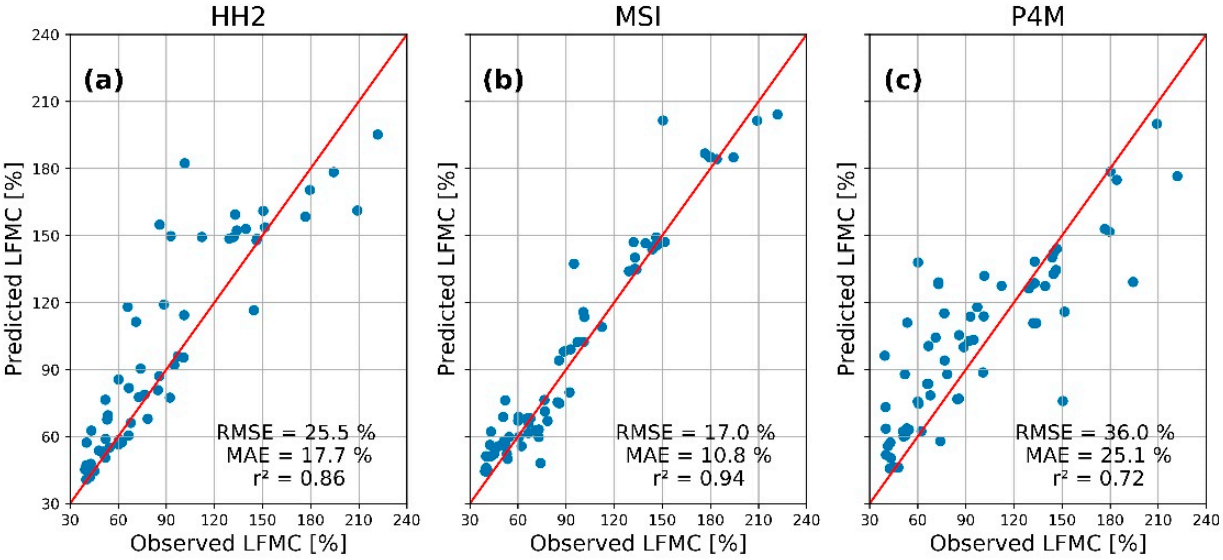

Figure 6. RF model evaluation between observations and predicted for LFMC values based on (**a**) HH2, (**b**) MSI and (**c**) P4M sensors. The red line denotes a 1:1 relationship.

3.4. Final Remarks

This study shows an intercomparison analysis between reflectance measurements obtained by each sensor with different scales over shrubland areas in Portugal. The sensors used were P4M camera onboard an UAV flying at 120 m height providing a 6 cm spatial resolution imagery, MSI carried by Sentinel-2 satellite which provides 10–60 m spatial resolution imagery, and a fully visible-near infrared spectrum retrieved by HH2 field spectroradiometer sensor.

The P4M sensor's camera includes red and infrared channels, allowing the internal software to automatically obtain NDVI information. Nevertheless, it is crucial to use a calibrated reflectance panel, which converts the digital number into surface reflectance, enabling intercomparison measurement with other sensors. Without this panel, it would not be possible to carry out these kinds of experiments. It is important to highlight that even with only 5 bands, P4M can estimate the vegetation live fuel moisture content satisfactorily. Furthermore, P4M could be used in studies where high resolution is needed, since UAVs have the capabilities to produce maps at sub-metric scale.

4. Conclusions

This work attempts to investigate how different multiple spatial and spectral scales, based on remote sensing observations, affect the reflectance signal and consequently, the LFMC estimates through machine learning techniques. This kind of work requires a great effort given the need for data acquisition planning organization, that is sometimes not available due to technical issues. This work provides useful information about how different spatial scales are important in understanding vegetation parameters.

This kind of intercomparison research between different sensors is crucial since the variability between data can be enormous depending on the target and local to be studied. This study has 1-year fieldwork campaigns that allowed the evaluation of vegetation spectral reflectance intra-annual variability. However, the interannual evaluation was very difficult due to the long-term information not contemplated in this work. As future work, the continuity of the fieldwork campaigns will allow increase the database information and enable an understanding of interannual variability.

Author Contributions: Conceptualization, F.L.M.S.; methodology, F.L.M.S.; software, F.L.M.S. and G.R.; validation, F.L.M.S.; formal analysis, F.L.M.S.; investigation, F.L.M.S. and G.R.; resources, F.L.M.S. and G.R.; data curation, F.L.M.S.; writing—original draft preparation, F.L.M.S.; writing—review and editing, G.R, M.P., F.T.C., M.J.C., S.D., M.J.M., N.d.A.R. and R.S.; visualization, F.L.M.S.; supervision, M.P., F.T.C., M.J.C. and R.S.; project administration, F.T.C. and R.S.; funding acquisition, F.T.C., M.J.C. and R.S. All authors have read and agreed to the published version of the manuscript.

Funding: Filippe L.M. Santos was supported by Portuguese Foundation for Science and Technology, I.P. (FCT), Grant Number (2022.11960.BD). The FCT also supported the work under the PyroC.pt project (Refs. PCIF/MPG/0175/2019), ICT project (Refs. UIDB/04683/2020 and UIDP/04683/2020). This research was co-funded by the European Union through the European Regional Development Fund (FEDER) in the framework of the Interreg VI-A España-Portugal (POCTEP) 2021–2027, FIRE-POCTEP+ (0139_FIREPOCTEP_MAS_6_E).

Data Availability Statement: Data is available on request for research purposes.

Acknowledgments: The authors thank Copernicus and European Space Agency for the data from Sentinel-2 provided to carry out this work.

Conflicts of Interest: The authors declare no conflicts of interest.

References

1. Bowman, D.M.J.S.; Kolden, C.A.; Abatzoglou, J.T.; Johnston, F.H.; van der Werf, G.R.; Flannigan, M. Vegetation Fires in the Anthropocene. *Nat. Rev. Earth Environ.* **2020**, *1*, 500–515. [CrossRef]
2. Flannigan, M.D.; Krawchuk, M.A.; de Groot, W.J.; Wotton, B.M.; Gowman, L.M. Implications of Changing Climate for Global Wildland Fire. *Int. J. Wildland Fire* **2009**, *18*, 483. [CrossRef]
3. Parente, J.; Pereira, M.G.; Amraoui, M.; Fischer, E.M. Heat Waves in Portugal: Current Regime, Changes in Future Climate and Impacts on Extreme Wildfires. *Sci. Total Environ.* **2018**, *631–632*, 534–549. [CrossRef] [PubMed]
4. Silva, P.; Carmo, M.; Rio, J.; Novo, I. Changes in the Seasonality of Fire Activity and Fire Weather in Portugal: Is the Wildfire Season Really Longer? *Meteorology* **2023**, *2*, 74–86. [CrossRef]
5. Couto, F.T.; Santos, F.L.M.; Campos, C.; Andrade, N.; Purificação, C.; Salgado, R. Is Portugal Starting to Burn All Year Long? The Transboundary Fire in January 2022. *Atmosphere* **2022**, *13*, 1677. [CrossRef]
6. Nunes, L.J.R.; Meireles, C.I.R.; Pinto Gomes, C.J.; Almeida Ribeiro, N.M.C. The Evolution of Climate Changes in Portugal: Determination of Trend Series and Its Impact on Forest Development. *Climate* **2019**, *7*, 78. [CrossRef]
7. Nunes, L.J.R.; Meireles, C.I.R.; Pinto Gomes, C.J.; Ribeiro, N.M.C.A. Socioeconomic Aspects of the Forests in Portugal: Recent Evolution and Perspectives of Sustainability of the Resource. *Forests* **2019**, *10*, 361. [CrossRef]
8. Yebra, M.; Dennison, P.E.; Chuvieco, E.; Riaño, D.; Zylstra, P.; Hunt, E.R.; Danson, F.M.; Qi, Y.; Jurdao, S. A Global Review of Remote Sensing of Live Fuel Moisture Content for Fire Danger Assessment: Moving towards Operational Products. *Remote Sens. Environ.* **2013**, *136*, 455–468. [CrossRef]
9. Couto, F.T.; Filippi, J.-B.; Baggio, R.; Campos, C.; Salgado, R. Triggering Pyro-Convection in a High-Resolution Coupled Fire–Atmosphere Simulation. *Fire* **2024**, *7*, 92. [CrossRef]
10. Ceccato, P.; Leblon, B.; Chuvieco, E.; Flasse, S.; Carlson, J.D. Estimation of Live Fuel Moisture Content. In *Wildland fire Danger Estimation and Mapping: The Role of Remote Sensing Data*; World Scientific: Singapore, 2003; pp. 63–90.
11. Yebra, M.; Scortechini, G.; Badi, A.; Beget, M.E.; Boer, M.M.; Bradstock, R.; Chuvieco, E.; Danson, F.M.; Dennison, P.; Resco de Dios, V.; et al. Globe-LFMC, a Global Plant Water Status Database for Vegetation Ecophysiology and Wildfire Applications. *Sci. Data* **2019**, *6*, 155. [CrossRef]
12. Yebra, M.; Scortechini, G.; Adeline, K.; Aktepe, N.; Almoustafa, T.; Bar-Massada, A.; Beget, M.E.; Boer, M.; Bradstock, R.; Brown, T.; et al. Globe-LFMC 2.0, an Enhanced and Updated Dataset for Live Fuel Moisture Content Research. *Sci. Data* **2024**, *11*, 332. [CrossRef] [PubMed]
13. Santos, F.L.M.; Couto, F.T.; Dias, S.S.; Ribeiro, N.d.A.; Salgado, R. Vegetation Fuel Characterization Using Machine Learning Approach over Southern Portugal. *Remote Sens. Appl.* **2023**, *32*, 101017. [CrossRef]
14. Costa-Saura, J.M.; Balaguer-Beser, Á.; Ruiz, L.A.; Pardo-Pascual, J.E.; Soriano-Sancho, J.L. Empirical Models for Spatio-Temporal Live Fuel Moisture Content Estimation in Mixed Mediterranean Vegetation Areas Using Sentinel-2 Indices and Meteorological Data. *Remote Sens.* **2021**, *13*, 3726. [CrossRef]
15. Fan, L.; Wigneron, J.-P.; Xiao, Q.; Al-Yaari, A.; Wen, J.; Martin-StPaul, N.; Dupuy, J.-L.; Pimont, F.; Al Bitar, A.; Fernandez-Moran, R.; et al. Evaluation of Microwave Remote Sensing for Monitoring Live Fuel Moisture Content in the Mediterranean Region. *Remote Sens. Environ.* **2018**, *205*, 210–223. [CrossRef]
16. Tanase, M.A.; Nova, J.P.G.; Marino, E.; Aponte, C.; Tomé, J.L.; Yáñez, L.; Madrigal, J.; Guijarro, M.; Hernando, C. Characterizing Live Fuel Moisture Content from Active and Passive Sensors in a Mediterranean Environment. *Forests* **2022**, *13*, 1846. [CrossRef]
17. Xing, J.; Wang, C.; Liu, Y.; Chao, Z.; Guo, J.; Wang, H.; Chang, X. UAV Multispectral Imagery Predicts Dead Fuel Moisture Content. *Forests* **2023**, *14*, 1724. [CrossRef]

18. Barber, N.; Alvarado, E.; Kane, V.R.; Mell, W.E.; Moskal, L.M. Estimating Fuel Moisture in Grasslands Using UAV-Mounted Infrared and Visible Light Sensors. *Sensors* **2021**, *21*, 6350. [CrossRef]
19. Madani, A.A.; Harbi, H.M.; El-Dougdoug, A.M.A.; Surour, A.A.; Ahmed, A.H. Spectral Characteristics of Listvenites and Serpentineites Along Ophiolite-Decorated Megashears (Suture Zones) in the Arabian Shield Using ASD Fieldspec and Satellite Data. In *The Geology of the Arabian-Nubian Shield*; Hamimi, Z., Fowler, A.-R., Liégeois, J.-P., Collins, A., Abdelsalam, M.G., Abd EI-Wahed, M., Eds.; Springer International Publishing: Cham, Switzerland, 2021; pp. 559–583.
20. Thomson, E.R.; Spiegel, M.P.; Althuizen, I.H.J.; Bass, P.; Chen, S.; Chmurzynski, A.; Halbritter, A.H.; Henn, J.J.; Jónsdóttir, I.S.; Klanderud, K.; et al. Multiscale Mapping of Plant Functional Groups and Plant Traits in the High Arctic Using Field Spectroscopy, UAV Imagery and Sentinel-2A Data. *Environ. Res. Lett.* **2021**, *16*, 055006. [CrossRef]
21. Lausch, A.; Pause, M.; Merbach, I.; Zacharias, S.; Doktor, D.; Volk, M.; Seppelt, R. A New Multiscale Approach for Monitoring Vegetation Using Remote Sensing-Based Indicators in Laboratory, Field, and Landscape. *Environ. Monit. Assess* **2013**, *185*, 1215–1235. [CrossRef]
22. Chen, Y.N.; Fan, K.C.; Chang, Y.L.; Moriyama, T. Special Issue Review: Artificial Intelligence and Machine Learning Applications in Remote Sensing. *Remote Sens.* **2023**, *15*, 569. [CrossRef]
23. Mutanga, O.; Masenyama, A.; Sibanda, M. Spectral Saturation in the Remote Sensing of High-Density Vegetation Traits: A Systematic Review of Progress, Challenges, and Prospects. *ISPRS J. Photogramm. Remote Sens.* **2023**, *198*, 297–309. [CrossRef]
24. Hou, X.; Wu, Z.; Zhu, S.; Li, Z.; Li, S. Comparative Analysis of Machine Learning-Based Predictive Models for Fine Dead Fuel Moisture of Subtropical Forest in China. *Forests* **2024**, *15*, 736. [CrossRef]
25. Schreck, J.S.; Petzke, W.; Jiménez, P.A.; Brummet, T.; Knievel, J.C.; James, E.; Kosović, B.; Gagne, D.J. Machine Learning and VIIRS Satellite Retrievals for Skillful Fuel Moisture Content Monitoring in Wildfire Management. *Remote Sens.* **2023**, *15*, 3372. [CrossRef]
26. Reif, D.M.; Motsinger, A.A.; McKinney, B.A.; Crowe, J.E.; Moore, J.H. Feature Selection Using a Random Forests Classifier for the Integrated Analysis of Multiple Data Types. In Proceedings of the 2006 IEEE Symposium on Computational Intelligence and Bioinformatics and Computational Biology, Toronto, ON, Canada, 28–29 September 2006; IEEE: New Jersey, NJ, USA, 2006; pp. 1–8.
27. Mancilla-Leytón, J.M.; Pino Mejías, R.; Martín Vicente, A. Do Goats Preserve the Forest? Evaluating the Effects of Grazing Goats on Combustible Mediterranean Scrub. *Appl. Veg. Sci.* **2013**, *16*, 63–73. [CrossRef]
28. Mitra-Nature: Biodiversidade da Herdade da Mitra Instituto Mediterrâneo Para a Agricultura, Ambiente e Desenvolvimento—Grupo de Investigação Ecologia Aplicada e Conservação, Universidade de Évora. Available online: http://www.mitra-nature.uevora.pt/ (accessed on 10 February 2023).
29. Pinto-Correia, T.; Ribeiro, N.; Sá-Sousa, P. Introducing the Montado, the Cork and Holm Oak Agroforestry System of Southern Portugal. *Agrofor. Syst.* **2011**, *82*, 99–104. [CrossRef]
30. Haase, S.M.; Sánchez, J.; Weise, D.R. *Evaluation of Standard Methods for Collecting and Processing Fuel Moisture Samples*; US Department of Agriculture, Forest Service, Pacific Southwest Research Station: Albany, CA, USA, 2016; Volume 268.
31. Santos, F.L.M.; Couto, F.T.; Dias, S.; Ribeiro, N.; Salgado, R. South Portugal Live Fuel Moisture Content (LFMC) Dataset. Available online: https://zenodo.org/doi/10.5281/zenodo.7254644 (accessed on 31 July 2024).
32. Main-Knorn, M.; Pflug, B.; Louis, J.; Debaecker, V.; Müller-Wilm, U.; Gascon, F. Sen2Cor for Sentinel-2. In Proceedings of the Image and Signal Processing for Remote Sensing XXIII, Warsaw, Poland, 11–14 September 2017; Volume 10427, pp. 37–48. [CrossRef]
33. Velastegui-Montoya, A.; Montalván-Burbano, N.; Carrión-Mero, P.; Rivera-Torres, H.; Sadeck, L.; Adami, M. Google Earth Engine: A Global Analysis and Future Trends. *Remote Sens.* **2023**, *15*, 3675. [CrossRef]
34. Potes, M.; Costa, M.J.; Salgado, R.; Bortoli, D.; Serafim, A.; Le Moigne, P. Spectral Measurements of Underwater Downwelling Radiance of Inland Water Bodies. *Tellus A Dyn. Meteorol. Oceanogr.* **2013**, *65*, 20774. [CrossRef]
35. Rodrigues, G.; Potes, M.; Penha, A.M.; Costa, M.J.; Morais, M.M. The Use of Sentinel-3/OLCI for Monitoring the Water Quality and Optical Water Types in the Largest Portuguese Reservoir. *Remote Sens.* **2022**, *14*, 2172. [CrossRef]
36. Breiman, L. Random Forests. *Mach. Learn.* **2001**, *45*, 5–32. [CrossRef]
37. Breiman, L.; Friedman, J.H.; Olshen, R.A.; Stone, C.J. *Classification and Regression Trees*; Routledge: London, UK, 2017; ISBN 9781315139470.
38. Pellizzaro, G.; Duce, P.; Ventura, A.; Zara, P. Seasonal Variations of Live Moisture Content and Ignitability in Shrubs of the Mediterranean Basin. *Int. J. Wildland Fire* **2007**, *16*, 633. [CrossRef]
39. Pellizzaro, G.; Cesaraccio, C.; Duce, P.; Ventura, A.; Zara, P. Relationships between Seasonal Patterns of Live Fuel Moisture and Meteorological Drought Indices for Mediterranean Shrubland Species. *Int. J. Wildland Fire* **2007**, *16*, 232. [CrossRef]
40. Ardilouze, C.; Materia, S.; Batté, L.; Benassi, M.; Prodhomme, C. Precipitation Response to Extreme Soil Moisture Conditions over the Mediterranean. *Clim. Dyn.* **2022**, *58*, 1927–1942. [CrossRef]
41. Viegas, D.X.; Piñol, J.; Viegas, M.T.; Ogaya, R. Estimating Live Fine Fuels Moisture Content Using Meteorologically-Based Indices. *Int. J. Wildland Fire* **2001**, *10*, 223. [CrossRef]
42. Benedetti, R.; Rossini, P. On the Use of NDVI Profiles as a Tool for Agricultural Statistics: The Case Study of Wheat Yield Estimate and Forecast in Emilia Romagna. *Remote Sens. Environ.* **1993**, *45*, 311–326. [CrossRef]
43. Serrano, J.; Shahidian, S.; Paixão, L.; Marques da Silva, J.; Morais, T.; Teixeira, R.; Domingos, T. Spatiotemporal Patterns of Pasture Quality Based on NDVI Time-Series in Mediterranean Montado Ecosystem. *Remote Sens.* **2021**, *13*, 3820. [CrossRef]

44. Meivel, S.; Maheswari, S. Remote Sensing Analysis of Agricultural Drone. *J. Indian Soc. Remote Sens.* **2021**, *49*, 689–701. [CrossRef]
45. Wang, L.; Qu, J.J.; Hao, X.; Zhu, Q. Sensitivity Studies of the Moisture Effects on MODIS SWIR Reflectance and Vegetation Water Indices. *Int. J. Remote Sens.* **2008**, *29*, 7065–7075. [CrossRef]